

Suppression of Prostate Cancer Nodal and Systemic Metastasis by Blockade of the Lymphangiogenic Axis

Jeremy B. Burton,¹ Saul J. Priceman,¹ James L. Sung,¹ Ebba Brakenhielm,^{2,4} Dong Sung An,³ Bronislaw Pytowski,⁵ Kari Alitalo,⁶ and Lily Wu^{1,2}

¹Department of Molecular and Medical Pharmacology, ²Department of Urology, ³Department of Medicine, and Jonsson Comprehensive Cancer Center, David Geffen School of Medicine, University of California Los Angeles, Los Angeles, California; ⁴Rouen Medical-Pharmacological University, Rouen, France; ⁵Department of Cell Biology, ImClone Systems, New York, New York; and ⁶Molecular Cancer Biology Laboratory and Ludwig Institute for Cancer Research, Biomedicum Helsinki, Haartman Institute and Helsinki University Central Hospital, University of Helsinki, Helsinki, Finland

Abstract

Lymph node involvement denotes a poor outcome for patients with prostate cancer. Our group, along with others, has shown that initial tumor cell dissemination to regional lymph nodes via lymphatics also promotes systemic metastasis in mouse models. The aim of this study was to investigate the efficacy of suppressive therapies targeting either the angiogenic or lymphangiogenic axis in inhibiting regional lymph node and systemic metastasis in subcutaneous and orthotopic prostate tumor xenografts. Both androgen-dependent and more aggressive androgen-independent prostate tumors were used in our investigations. Interestingly, we observed that the threshold for dissemination is lower in the vascular-rich prostatic microenvironment compared with subcutaneously grafted tumors. Both vascular endothelial growth factor-C (VEGF-C) ligand trap (sVEGFR-3) and antibody directed against VEGFR-3 (mF4-31C1) significantly reduced tumor lymphangiogenesis and metastasis to regional lymph nodes and distal vital organs without influencing tumor growth. Conversely, angiogenic blockade by short hairpin RNA against VEGF or anti-VEGFR-2 antibody (DC101) reduced tumor blood vessel density, significantly delayed tumor growth, and reduced systemic metastasis, although it was ineffective in reducing lymphangiogenesis or nodal metastasis. Collectively, these data clarify the utility of vascular therapeutics in prostate tumor growth and metastasis, particularly in the context of the prostate microenvironment. Our findings highlight the importance of lymphangiogenic therapies in the control of regional lymph node and systemic metastasis. [Cancer Res 2008;68(19):7828–37]

Introduction

Prostate cancer is the most common cancer among men and second in cancer-related deaths in the United States (1). Whereas monitoring serum PSA and histopathology (Gleason grade) are useful in clinical assessment, pelvic lymph node metastasis remains the most significant indicator of patient prognosis and determinant of therapeutic aggressiveness (2, 3). As prostate carcinoma

progresses, systemic metastasis to bone and liver ultimately lead to patient morbidity and mortality. Current treatments include radical prostatectomy, usually with pelvic lymphadenectomy for lymph node assessment, followed by radiation or hormone therapy (4). There are currently no effective treatments for recurrent or metastatic disease, highlighting the importance of alternative strategies for early intervention.

Angiogenesis is essential for the growth of solid cancers beyond 2 mm, which is the limit of nutrient diffusion (5). This process also clearly contributes to metastasis of most solid cancers. Vascular endothelial growth factor-A (VEGF-A) signaling through its receptor VEGFR-2 is critical for the development and maintenance of tumor blood vasculature (6, 7). Inhibition of VEGF signaling, by targeting either the ligand or the receptor, suppresses both tumor growth and metastasis and is currently being tested in clinical trials as single agents and in combination with chemotherapy or radiation therapy (6, 8, 9). More recently, lymphangiogenesis has received much attention as an important mediator of tumor cell dissemination. VEGF-C and VEGF-D, the major lymphangiogenic ligands for the receptor VEGFR-3, induce proliferation of lymphatic endothelial cells and sprouting of lymphatic vessels (10, 11). VEGFR-3-mediated lymphangiogenesis also potently influences lymph node metastasis in various tumor models (12–14). Recent studies by our group and others have also provided evidence for the direct contribution of VEGF to lymphangiogenesis, in addition to its principal functions in angiogenesis (15–17). Overall, targeting of the VEGFR-2 and VEGFR-3 signaling pathways are promising therapies for the treatment of solid cancers.

In prostate cancer, the expression of VEGF-C and VEGFR-3 has been shown to be highly associated with regional lymph node metastasis (18–21). Our previous studies have correlated the levels of tumor-derived VEGF-C with the extent of tumor lymphatics and subsequent lymph node and lung metastases in xenograft models of human prostate cancer (22). The precise contributions of intratumoral and peritumoral lymphatics to lymph node metastasis have been extensively debated and require further investigation (23). Recent reports have highlighted that lymphogenous spread can augment systemic metastasis (22, 24). Although angiogenesis and lymphangiogenesis are critical mediators of the metastatic process, the distinct contributions of each axis to nodal and systemic metastasis of prostate cancer remain unclear.

In the current study, we used VEGF or VEGF-C pathway-specific therapies to decipher their roles in lymph node and lung metastasis of prostate cancer. Using overexpression and short hairpin RNA (shRNA) silencing of these growth factors, we show that VEGF-C and, to a lesser extent, VEGF are required for lymph node and subsequent lung metastasis. Furthermore, the findings from using

Note: Supplementary data for this article are available at Cancer Research Online (<http://cancerres.aacrjournals.org/>).

J.B. Burton and S.J. Priceman contributed equally to this work.

Requests for reprints: Lily Wu, Department of Urology, MRL 2210, Box 951738, University of California, Los Angeles, CA 90095-1738. Phone: 310-825-8511; Fax: 310-206-5343; E-mail: LWu@mednet.ucla.edu.

©2008 American Association for Cancer Research.
doi:10.1158/0008-5472.CAN-08-1488

specific inhibitors of the VEGFR-2 and VEGFR-3 axes indicate that, in prostate cancer, angiogenesis plays a critical role in prostate tumor growth and systemic metastasis, but targeting the VEGFR-2 axis alone does not significantly reduce tumor lymphangiogenesis or nodal metastasis. However, targeting the lymphangiogenic axis significantly reduces both lymph node and systemic metastasis in our model, without significantly influencing primary tumor growth. Consequently, we believe that combination treatments targeting both vascular axes in conjunction with conventional therapy may offer the best protection against recurrent, disseminated disease in prostate cancer patients with a poor prognosis.

Materials and Methods

Tumor cells. The androgen-independent, androgen-responsive CWR22Rv-1 tumor cell line (kind gift from Dr. David Agus, Cedars-Sinai Medical Center) was maintained *in vitro* in RPMI containing 10% fetal bovine serum (FBS) and 1% penicillin/streptomycin. The androgen-dependent human prostate cancer cell line LAPC-9 was a kind gift from Dr. Charles Sawyers (Memorial Sloan Kettering Cancer Center). LAPC-9 xenografts were maintained *in vivo* and manipulated *ex vivo*, as previously described (22).

Lentiviral production and tumor cell transduction. For all *in vivo* studies, cells were transduced using lentivirus carrying cytomegalovirus (CMV) promoter-driven *Renilla* luciferase (RL) reporter genes, as previously described (22). For overexpression studies, tumor cells were transduced with lentiviral vector pCCL-CMV-VEGF-C-IRES-EGFP (VEGF-C), pCCL-CMV-VEGF-C_{C156S}-IRES-EGFP (VEGF-C_{C156S}), pCCL-CMV-VEGF-IRES-EGFP (VEGF), pCCL-CMV-sVEGFR-3-IRES-EGFP (sVEGFR-3), or empty vector control pCCL-CMV-IRES-EGFP (Ctrl). For shRNA studies, CWR22Rv-1 cells were transduced with pRRL-U6polIII-VEGF-A-shRNA-PGKp-EGFP (shVEGF-A) or an identical vector replacing VEGF-A shRNA with irrelevant shRNA against firefly luciferase. Tumor cells were infected using viral supernatant at multiplicity of infection (MOI) of 1 during 6 h incubation. Cellular expression of *Renilla* was confirmed using an *in vitro* bioluminescence assay (Promega).

shRNA interference constructs. Short hairpin constructs were generated and tested, as described previously (25), using the vegf-a target sequence CATCACCATGCAGATTATG. Before generating lentiviral vectors, pRRL-vectors were tested by transient transfection in 24-well cell culture dishes. Briefly, DNA vectors were transfected into CWR22Rv-1 cells using Lipofectamine 2000 reagent according to manufacturer's instructions (Invitrogen). Specific silencing capabilities were determined at the transcription and translation levels. Candidate shRNAs were subcloned under the U6polIII promoter in pRRL-U6polIII-PGKp-EGFP.

Real-time reverse transcription-PCR analysis. Total cellular RNA was extracted from cell lines using Tri Reagent (Sigma Aldrich). RNA was isolated according to the TRIzol procedure. RNA was quantified and assessed for purity by UV spectrophotometry and gel electrophoresis. RNA (1 µg) was reverse-transcribed using the TaqMan Reverse Transcription Reagent kit (Applied Biosystems) according to manufacturer's instructions. The real-time PCR method and primer sequences were previously described (22).

Western blot and ELISA assays. Cell lysates were prepared from cells infected with lentiviral vectors described above using ice-cold radioimmunoprecipitation assay lysis buffer containing protease inhibitor cocktail (Sigma-Aldrich). Protein lysates (50 µg) were separated by SDS-PAGE and transferred to a polyvinylidene difluoride membrane. Membranes were probed using antibodies specific for human VEGFR-3 (R&D Systems), human VEGF-A (R&D Systems), or β-actin (Sigma-Aldrich), followed by horseradish peroxidase-conjugated anti-IgG and detected using an enhanced chemiluminescence kit (Amersham). For ELISA, cells were serum-starved with RPMI media containing 0.1% FBS overnight. Cell supernatants were collected after a 24-h incubation. Human VEGF-A and VEGF-C concentrations were determined using the respective Quantikine ELISA assay (R&D Systems) according to manufacturer's instructions.

Before implanting cells, LAPC-9 supernatants were collected and analyzed by ELISA and Western blot to ensure equivalent expression levels.

Noninvasive and *ex vivo* imaging. CWR22Rv-1 cells (5×10^5) were implanted subcutaneously above the right shoulder of immunodeficient SCID/*beige* male mice (Taconic). Tumor size was measured regularly using digital calipers and by noninvasive optical imaging as follows. After administration of *Renilla* luciferase substrate, coelenterazine (1 mg/kg i.v.), anaesthetized mice (i.p. injection of a 4:1 mixture of ketamine and xylazine) were imaged as previously described (22). Primary tumors were grown to the ethical limit of 1.5 cm in diameter, at which time the animals were sacrificed.

For orthotopic implants, transduced CWR22Rv-1 cells (1×10^5) or LAPC-9 cells (2.5×10^5) suspended in Matrigel were implanted in the surgically exposed prostate region of SCID/*beige* male mice, as previously described (26). Cells (in 10 µL/lobe) were implanted at the base of the exposed seminal vesicles in each dorsolateral lobe. Incisions were closed with vicryl sutures (Novartis) and tumor growth was monitored optically over the course of the next 3 wk.

Micro-computed tomography contrast imaging. Tumor-bearing mice were anesthetized and Fenesta vascular contrast (Alerion) agent was injected i.v. into the tail vein and imaged after 1 h. One representative animal from the control and experimental group was used for vascular contrast computed tomography (CT) imaging. Mice were imaged with a micro-CT scanner (MicroCAT II, Siemens Preclinical Solutions) over 7 min using 70 kVp, 500-ms exposures, and 360° rotation to create images with 200-µm voxel size. CT datasets were analyzed using AMIDE software (27).

Therapeutic antibodies. Monoclonal antibodies raised against mouse VEGFR-2 (DC101) and mouse VEGFR-3 (mF4-31C1) were generated by ImClone Systems (28, 29). CWR22Rv-1 cells were implanted orthotopically as described above, and mice were randomly assigned to each of the treatment groups. Therapeutic antibodies were given i.p. at 800 µg/mouse every other day, beginning 3 d after tumor implantation. Treatments continued until mice were sacrificed at tumor threshold.

Immunohistochemistry. Tumors, lymph nodes, and lungs were harvested and fixed in 3% paraformaldehyde overnight. Sections (5 µm) were stained with anti-Lyve-1 (RELIAtech) or anti-CD31 (BD Biosciences) antibodies, as previously described (22). Images were processed and quantified as previously described (30). Lymphatic vessels extending into the tumor margin were classified as intratumoral lymphatics, whereas those lacking contact with tumor cells were considered peritumoral. For orthotopic implants, Lyve-1+ lymphatics in the prostate region outside of the tumor margin were used in the quantification of Lyve-1+ vessel density.

Results

Induction of angiogenesis and lymphangiogenesis in the subcutaneous LAPC-9 prostate tumor model. In our experience, the androgen-dependent PSA+ and AR+ LAPC-9 (31) human prostate tumor is an excellent model to study the influence of vascular growth factors on metastasis. Subcutaneously implanted LAPC-9 tumors displayed inherently low metastatic potential with few intratumoral and peritumoral lymphatics (22). However, induced expression of VEGF-C in this tumor model to a level >2-fold higher than PC-3 prostate xenografts resulted in dramatic enhancement of intratumoral lymphangiogenesis and subsequent lymphatic metastasis (22). To further distinguish the relative roles of the lymphatic and blood vasculature in metastasis, we compared, in parallel, the effects of overexpressing VEGF, VEGF-C_{C156S}, or VEGF-C in LAPC-9 tumors. The VEGF-C_{C156S} gene is a lymphatic-specific variant that lacks the angiogenic VEGFR-2 stimulatory activity of VEGF-C (32).

The tumoral blood and lymphatic vascular densities were assessed by anti-CD31 or anti-Lyve-1 staining, respectively (Fig. 1A). Overexpression of VEGF and VEGF-C enhanced blood vessel density by 3-fold or 2-fold over control tumors, respectively,

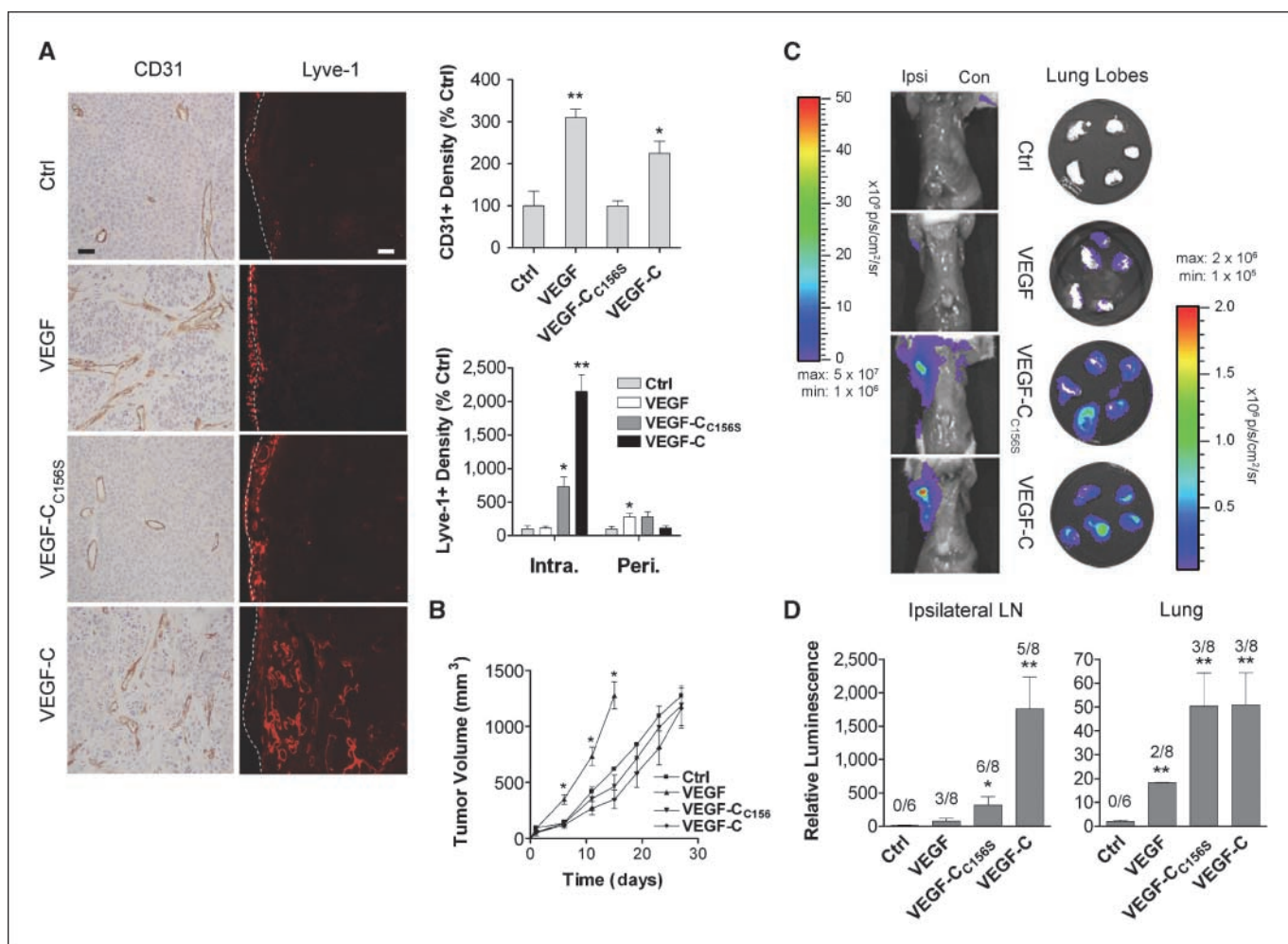


Figure 1. Induction of angiogenesis and lymphangiogenesis in the subcutaneous LAPC-9 prostate tumor model. SCID/*beige* mice were implanted with LAPC-9 tumor cells expressing *Renilla* luciferase and the respective growth factor (VEGF-A, VEGF-C, VEGF-C_{C156S}, or empty vector control). **A**, tumors were fixed, sectioned, and stained with antibodies recognizing blood vessels (*CD31*) and lymphatic vessels (*Lyve-1*). Blood vessels were distributed throughout the tumor section, whereas lymphatics were predominantly in the tumor margin (tumor edge is marked by white dotted line). Vessel quantification was performed from at least five representative areas from each tumor for CD31+ blood vessels (*CD31*) and Lyve-1+ lymphatic vessels (*Lyve-1*). Overall counts were normalized by area and represented as a percentage compared with control. **B**, tumor growth was monitored by caliper measurements every 4 d once tumors became palpable (length × width × 0.52). When tumors reached ethical size limit, animals were sacrificed and skin was peeled back to expose regional axillary lymph nodes. **C**, representative images of animals from each group revealed photon emission in the ipsilateral, but not in contralateral, axilla. Lungs were dissected into separate lobes and imaged. **D**, bioluminescent signals from ipsilateral lymph node (LN) or lung of all animals in a cohort were averaged and normalized to background luminescence. The number of animals in each cohort that displayed significant metastasis by bioluminescent signals is listed above each bar. Optical scale bars are in photons/s/cm²/steradian (p/s/cm²/sr) and histology bar represents 20 μ m. *, $P < 0.05$; **, $P < 0.01$; bars, \pm SE; $n = 6-8$.

whereas no significant change was observed in the VEGF-C_{C156S} overexpressing tumors. Although elevated lymphangiogenesis can be appreciated in all three groups, the localization of the Lyve-1+ vessels was distinct. The VEGF-C overexpressing tumors displayed the most dramatic increase (20-fold) in intratumoral lymphatic density, extending to depths of 1 mm within the tumor parenchyma in some regions, without an apparent increase in peritumoral lymphatics. In the VEGF-C_{C156S} overexpressing tumors, a 6-fold increase in intratumoral lymphatics was observed; however, the majority of lymphatics in the VEGF-C_{C156S} group remained in the tumor margin. These lymphatics were surrounded by tumor cells but failed to form vascular networks at depths >100 μ m. These results show the important differences in the vascular architecture induced by VEGF and VEGF-C in prostate cancer.

In accordance with differences in tumoral angiogenesis, the vascular growth factors exerted differential effects on LAPC-9

tumor growth (Fig. 1B). The VEGF tumors exhibited faster growth, as they reached ethical size limit (1.5 cm in diameter) within 15 days, which is significantly faster than the control tumors at 27 days. There was no significant enhancement in the growth rate of the VEGF-C or VEGF-C_{C156S} overexpressing tumors. These data show that in our prostate cancer model, VEGF/VEGFR-2 signaling contributes to tumor growth kinetics, whereas VEGF-C/VEGFR-2 and VEGF-C/VEGFR-3 signaling axes do not.

Next, we measured the magnitude of metastasis in each group by *ex vivo* optical imaging. Metastases were quantified when the primary tumor reached 1.5 cm in diameter. The *Renilla* luciferase bioluminescent signal of the transduced tumor cells enabled us to quantify and compare the volume of metastasis in the ipsilateral axillary lymph nodes *in situ* or in the dissected lung lobes in each animal (Fig. 1C). Lymph nodes from the control group displayed bioluminescent signal at \sim 15-fold above background luminescence. By comparison, the VEGF-C_{C156S} and VEGF-C overexpressing

groups revealed dramatically higher ipsilateral axillary lymph node signals, averaging 300-fold in six of eight mice and 1,750-fold above background in five of eight mice, respectively (Fig. 1D). Three of eight mice in the VEGF overexpressing group also displayed elevated signal in the ipsilateral lymph node, but the intensity was ~4-fold and 10-fold lower than that of VEGF-C and VEGF-C_{C156S}, respectively. Interestingly, VEGF-C_{C156S} and VEGF-C induced lung metastasis to similar levels (~50-fold above background), which was higher than that of VEGF (18-fold). Moreover, significant metastatic lung signals were observed only in animals with lymph node metastasis, suggesting that lymph node metastasis facilitates systemic spread. It is unclear why VEGF-C_{C156S} had reduced lymphangiogenic effect, although the resulting difference highlights the importance of invasive lymphangiogenesis in metastasis, quantitatively and/or temporally. Collectively, these results suggest that lymphangiogenesis, and not angiogenesis, plays a dominant role in lymph node metastasis.

VEGF-C contributes to lymph node and systemic metastasis of the subcutaneous CWR22Rv-1 prostate tumor model. In our prior survey of several human prostate xenograft models, the androgen-independent, PSA+ and AR+ CWR22Rv-1 model displayed aggressive and metastatic growth *in vivo* (22, 33). Hence, we next investigated the influence of enhancing and suppressing lymphangiogenesis in this more aggressive model. CWR22Rv-1 cells expressing *Renilla luciferase* (CWR/RL) were transduced with either lentivirus encoding VEGF-C, sVEGFR-3, or empty vector

control. Elevated VEGF-C levels were confirmed by real-time reverse transcription-PCR (RT-PCR; Supplementary Fig. S1A) and ELISA (Supplementary Fig. S1B) from cultured cells. No changes in VEGF-D expression were observed in response to VEGF-C overexpression (Supplementary Fig. S1A). CWR22Rv-1 tumor growth rate was not significantly enhanced in response to overexpression of VEGF-C compared with control (Fig. 2A). A significant delay in the growth rate was observed in the sVEGFR-3 overexpressing group, although tumor growth seemed to rebound exponentially after day 16. Control tumors displayed moderate lymphatic density, with peritumoral Lyve-1+ vessels extending into the tumor margin (Fig. 2B). Scattered intratumoral lymphatic vessels, closely associated with some blood vessels, were also observed in the control tumors. VEGF-C overexpression resulted in a dramatic influx of lymphatic vessels intratumorally with reduced peritumoral lymphatic density. Intratumoral vessels were more numerous and convoluted. Conversely, sVEGFR-3 expression reduced both peritumoral and intratumoral lymphatics. Angiogenesis was slightly elevated by VEGF-C overexpression and suppressed by sVEGFR-3, although these trends were not statistically significant. The slight inhibition on tumor blood vasculature by sVEGFR-3 could likely be responsible for the delay in tumor growth *in vivo*, as there were no differences in the growth rate of each group in cell culture (data not shown).

The magnitude of CWR/RL metastasis to brachial and axillary lymph nodes and lungs was measured by *ex vivo* bioluminescence

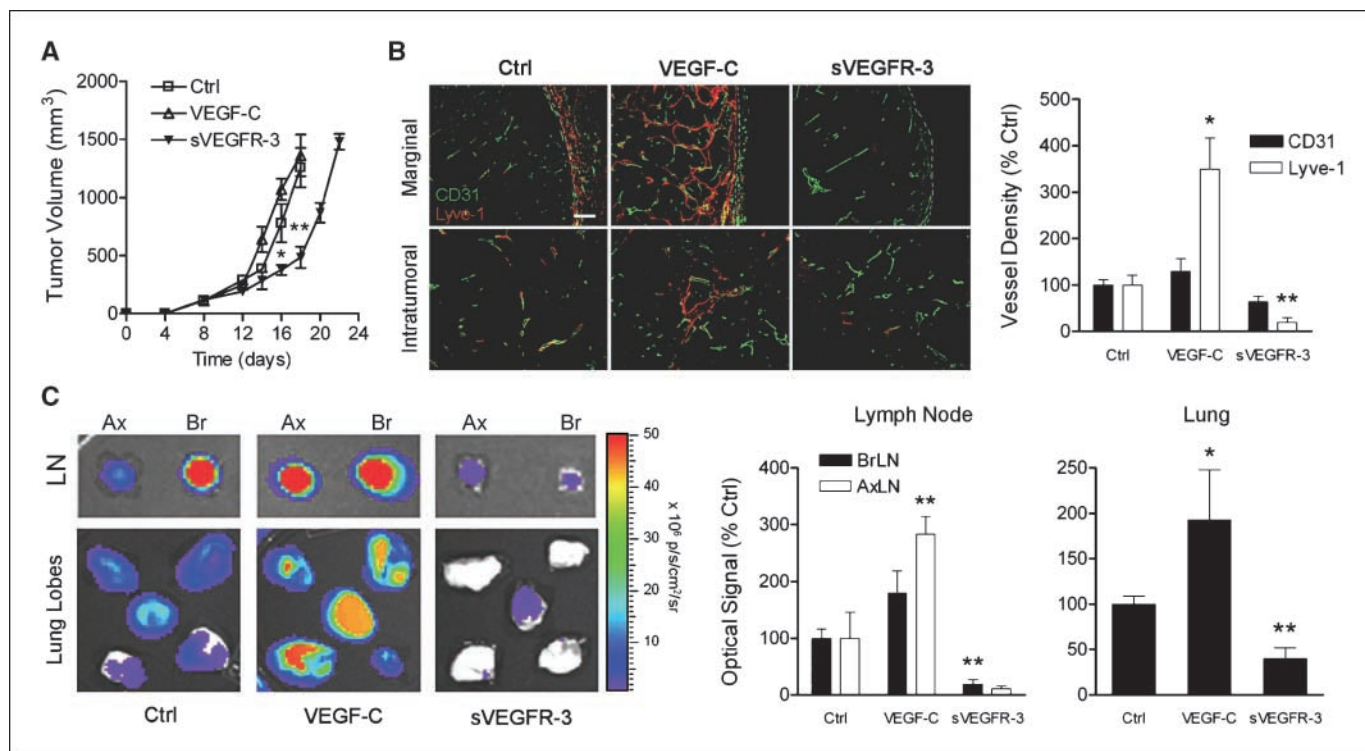


Figure 2. Intratumoral lymphangiogenesis in subcutaneous implants of CWR22Rv-1 is modulated by VEGF-C signaling. *A*, CWR22Rv-1 tumor cells expressing VEGF-C or sVEGFR-3 or empty vector (*Ctrl*) were implanted in SCID/*beige* mice, and tumor volume was monitored by caliper measurements until tumors reached ethical size limit. *B*, representative tumor sections displaying the tumor margin (white dotted line) delineating the intratumoral and peritumoral lymphatics (Lyve-1, red) and blood vessels (CD31, green) in CWR22Rv-1 tumors expressing the respective proteins. *Bottom*, representative sections displaying the intratumoral Lyve-1+ and CD31+ vasculature. Intratumoral (left of dotted line) Lyve-1+ and CD31+ areas were quantified for all tumors in each group (*n* = 4) and presented as percentage control. No significant differences in CD31 vessel density were detected. *C*, *ex vivo* optical signal was detected in indicated organs from representative animals (Ax, axillary; Br, brachial; lung). Bioluminescent signal intensity from each tissue was averaged for all animals in each group (graphs, lymph node and lung). *Histology scale bar*, 20 μ m. *Bars*, \pm SE. *, *P* < 0.05; **, *P* < 0.01.

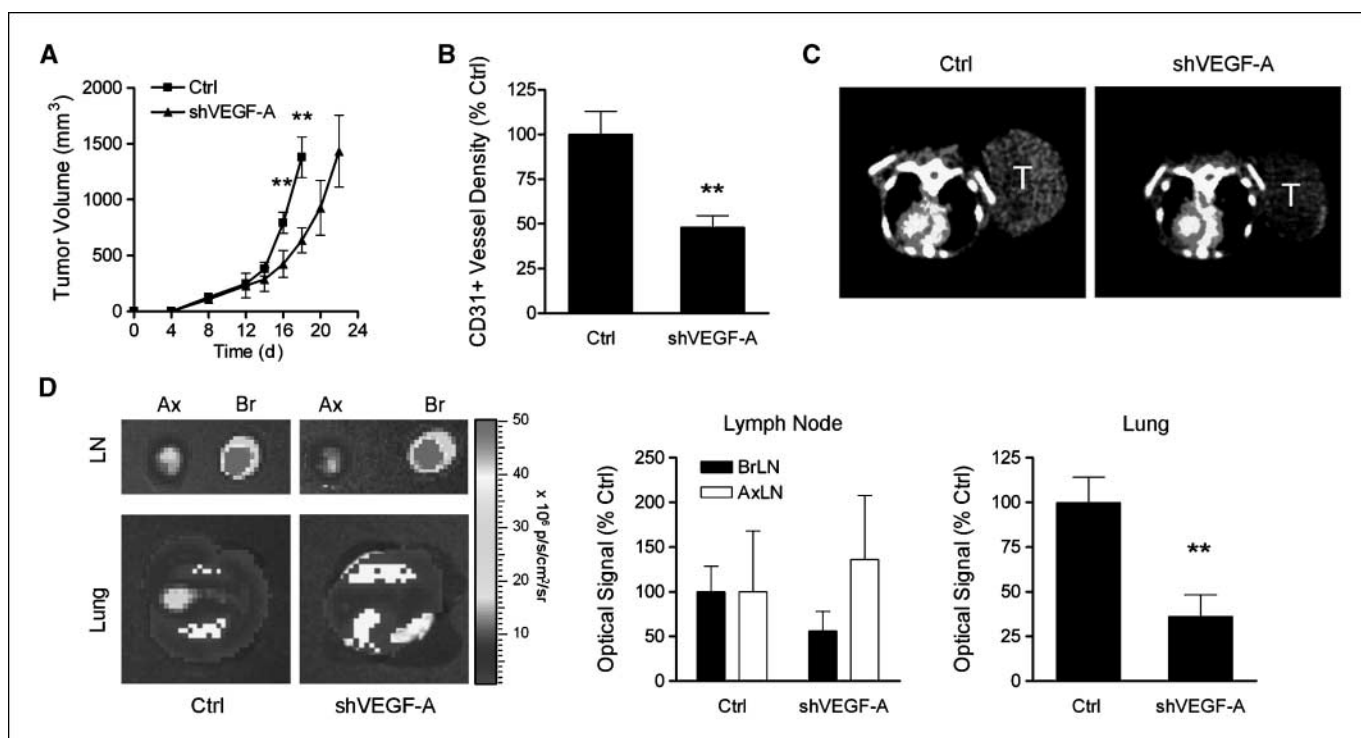


Figure 3. VEGF-A shRNA reduces tumor growth, blood vessel density, and systemic metastasis, without effecting lymph node metastasis. CWR22Rv-1 cells (5×10^5) transduced with lentivirus-expressing shRNA directed against firefly luciferase (*Ctrl*) or VEGF-A (*shVEGF-A*) were implanted subcutaneously on the shoulder of SCID/*beige* mice, and tumor volume was monitored. **A**, delay in tumor growth was observed in the shVEGF-A group. **B**, histologic analysis of tumor sections revealed 50% reduction in CD31+ tumor vasculature. **C**, micro-CT analysis using Fenestra vascular agent in representative animals revealed a reduction in contrast agent accumulation in the tumor (T) despite similar accumulation within the heart (center). **D**, after sacrifice and dissection, *ex vivo* optical signal was detected in indicated organs from representative animals (Ax, axillary LN; Br, brachial LN; lung). Maximum bioluminescent signal intensity from each tissue was averaged for all animals in each group and represented in the respective graph (lymph node and lung). Optical scale bars are in p/s/cm²/sr; bars, \pm SE. $n = 4$. **, $P < 0.01$.

signals (Fig. 2C). Compared with the control group, overexpression of VEGF-C resulted in an increase in disseminated tumor cells to regional lymph nodes and lung. In particular, VEGF-C overexpression enhanced dissemination to brachial and axillary nodes by 1.8-fold and 2.8-fold, respectively. Spread of tumor cells to the lung was also enhanced with VEGF-C overexpression by 1.9-fold. Conversely, the blockade of VEGF-C signal with sVEGFR-3 resulted in a significant reduction in dissemination to regional lymph nodes and lung to <20% and <50% of control, respectively. These results show the significant contribution of the VEGF-C/VEGFR-3 axis to regional lymph node and lung metastasis in the aggressive androgen-independent CWR22Rv-1 prostate cancer model.

Inhibition of VEGF signaling suppresses primary tumor growth and lung metastasis. Next, we sought to investigate the relative influence of the VEGF/VEGFR-2 axis in the CWR22Rv-1 prostate model. To this end, we generated lentivirus expressing shRNA against VEGF (*shVEGF-A*) under the U6 pol III promoter (25). Lentivirus expressing shRNA against the irrelevant firefly luciferase gene was used as a control (*Ctrl*). When CWR/RL cells were transduced with the respective shRNA lentiviral vectors at a MOI of 1, VEGF mRNA and secreted protein were reduced by 75% and 66%, respectively, as measured by real-time RT-PCR, ELISA, and Western blot (Supplementary Fig. S1C and D). There was no significant influence on VEGF-C expression in *shVEGF-A*-expressing cells compared with control.

The primary tumor growth rate of *shVEGF-A*-expressing tumors was significantly reduced compared with control (Fig. 3A). Staining of tumor sections revealed a 50% reduction in CD31+ blood vessel

density in *shVEGF-A*-expressing tumors (Fig. 3B). There was no difference in lymphatic vasculature between *Ctrl* and *shVEGF-A* (data not shown). The reduction in angiogenesis was also observed by comparing the relative uptake of the vascular contrast agent Fenestra by micro-CT analysis (Fig. 3C). Note that, whereas the Fenestra contrast uptake was normalized to the levels in the heart in both animals, the signal was significantly reduced throughout the *shVEGF-A*-expressing tumor.

We next asked whether a reduction in angiogenesis with *shVEGF-A* would reduce metastasis. VEGF knockdown had little influence on lymph node metastasis compared with control, although there was >50% reduction in tumor signal in the lung (Fig. 3D). This decreased signal in the lung likely represents the direct contribution of the tumor blood vasculature to systemic dissemination, although reduced angiogenesis and growth potential at the distal metastatic site are also possible explanations. Importantly, metastasis was quantified when each tumor volume reached the ethical threshold, ruling out the possibility that primary tumor size influenced metastatic behavior. Collectively, these data show an important role for VEGF in tumor growth and systemic metastasis, with minimal contributions to nodal metastasis in our model.

Blocking tumor lymphangiogenesis in orthotopic LAPC-9 tumors reduces lymph node metastasis. The stromal environment of the tumor can readily influence its metastatic behavior (34). For instance, subcutaneous LAPC-9 xenografts, in the absence of lymphangiogenic stimulus, exhibited low metastatic potential (Fig. 1; ref. 22). Conversely, when LAPC-9 tumors are implanted in

the blood and lymphatic vasculature-rich environment of the mouse prostate gland, we detected a propensity for nodal metastasis even in the absence of added lymphangiogenic drive (Fig. 4; ref. 44). Therefore, we assessed the effect of suppressing lymphangiogenesis on tumor dissemination from orthotopically

implanted LAPC-9/RL tumors. LAPC-9 tumor cells were transduced with lentiviral vectors containing either empty vector or sVEGFR-3. Repetitive optical imaging revealed comparable tumor growth rates between the control and sVEGFR-3 group (Fig. 4A). Nodal involvement in the periaortic and mesenteric lymph nodes

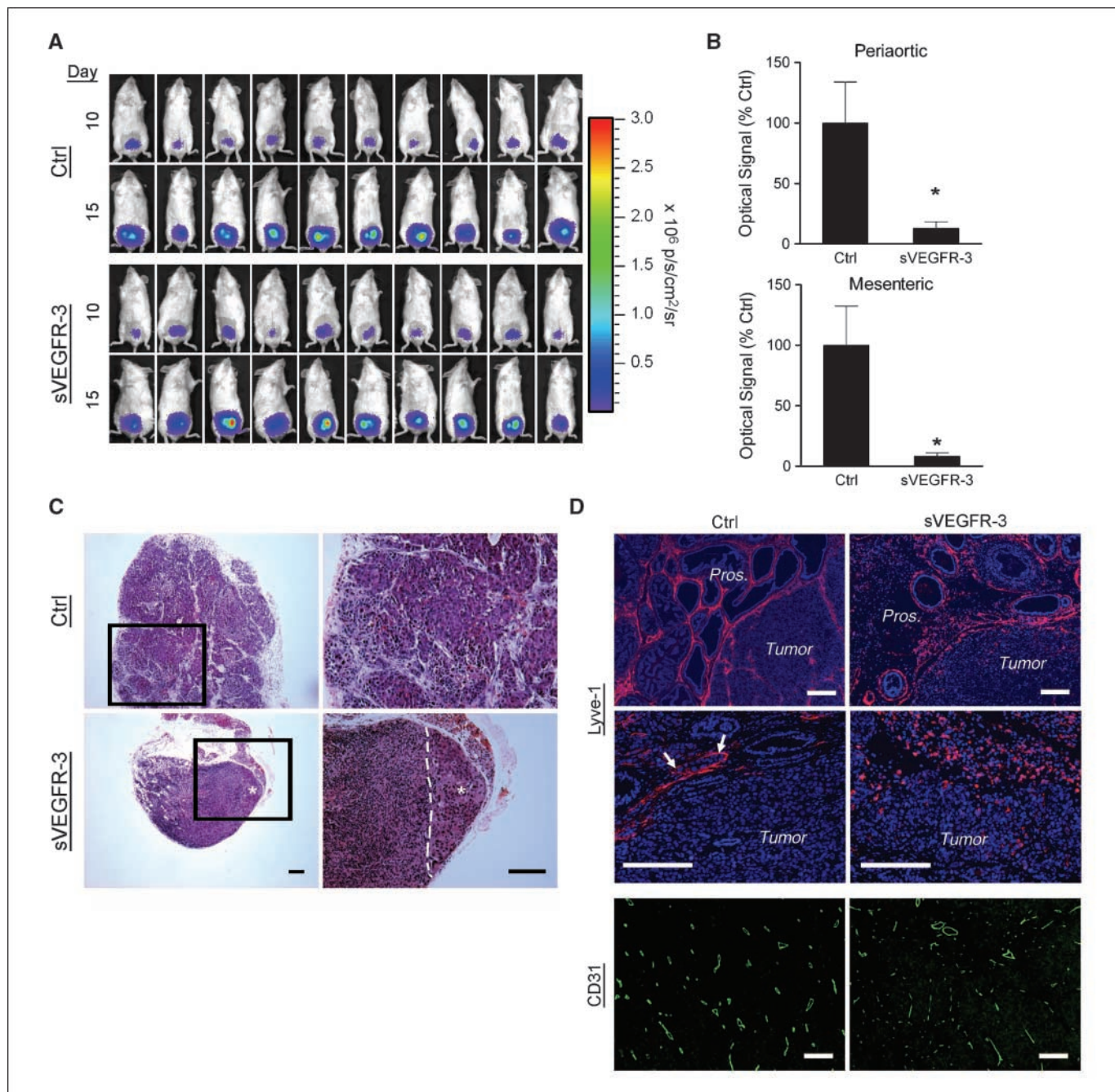


Figure 4. sVEGFR-3 reduces metastasis to regional lymph nodes in orthotopic LAPC-9 tumors. *A*, tumor-mediated optical signal (Ctrl, LAPC-9/RL/GFP; sVEGFR-3, LAPC-9/RL/sVEGFR-3/GFP) in all mice ($n = 10$ per group) shown during exponential growth phase at days 10 and 15 after orthotopic implantation. *B*, on day 16, mice were sacrificed and periaortic and mesenteric lymph nodes were removed and imaged *ex vivo* for *Renilla* luciferase activity. *C*, histologic analysis of H&E-stained sections revealed the presence of extensive metastasis throughout the periaortic lymph nodes of mice from control group (Ctrl), whereas lymph nodes from mice bearing sVEGFR-3 overexpressing tumors showed reduced metastasis (images to the right represent higher magnifications encompassed by the boxes). *D*, LAPC-9 tumors were fixed, paraffin-embedded, and sectioned through the junction of the seminal vesicles to reveal the interface of the prostate, seminal vesicle, and tumor xenograft. Lyve-1+ lymphatics (red) around the tumor margin and extending into the tumor were more profound in the controls compared with the punctate, disorganized lymphatics surrounding tumors expressing sVEGFR-3 (top). Higher magnification revealed the presence of numerous marginal lymphatics (often containing tumor cells, white arrow) in the control group (middle). No difference was observed in intratumoral angiogenesis between control and sVEGFR-3, as indicated by CD31 staining (bottom). Pros., prostate. Optical scale bars are in p/s/cm²/sr. Histology scale bar, 100 μ m (C) and 20 μ m (D). Bars, SE. *, $P < 0.05$.

was assessed by using *ex vivo* bioluminescence imaging to detect the presence of tumor cells in the harvested lymph nodes (Fig. 4B). Compared with control, metastasis to periaortic and mesenteric lymph nodes was reduced by 7-fold and 12-fold by sVEGFR-3, respectively. Histologic analysis of lymph node sections from the control group confirmed the presence of extensive tumor infiltration (Fig. 4C). The sVEGFR-3 group had minimal lymph node infiltration, although small subcapsular/parenchymal lesions were observed in about half of all the lymph nodes examined. No detectable lung metastasis was observed in either group in this study.

To examine the effect of sVEGFR-3 on tumor vasculature, we scrutinized the interface between the normal prostate region and the tumor. Control LAPC-9 tumors had extensive networks of Lyve-1+ lymphatic vessels extending throughout the normal prostate ductiles. These networks clearly aggregated around the tumor margin and extended into the tumor (Fig. 4D). Higher magnification revealed lymphatic vessels at the tumor margin intimately associated with tumor cells, which seemed to envelope some tumor cells in areas (Fig. 4D; *middle, white arrows*). By contrast, the sVEGFR-3-expressing tumors displayed different morphologic characteristics in their lymphatic vasculatures. In the tumor adjacent to the normal prostatic tissues, the lymphatic networks were less elaborate and discontinuous compared with the control group. In the tumor periphery, the Lyve-1+ structures were punctate and often seemed to be isolated cells, without contiguous vessels extending into the tumor margin. Depending on proteolytic processing, VEGF-C can also influence angiogenesis by directly binding to VEGFR-2 (35). Therefore, we also examined the influence of sVEGFR-3 on vascular density by comparing CD31 staining. We found no significant differences in the blood vessel density between control and sVEGFR-3-expressing tumors (Fig. 4D, *bottom*). These data suggest that sVEGFR-3 expression effectively suppressed VEGF-C and/or VEGF-D mediated lymphangiogenesis, as well as lymph node metastasis, from the prostatic microenvironment.

Effects of antibody-mediated VEGFR-2 and VEGFR-3 blockade on tumor growth and metastasis in orthotopic CWR22Rv-1 tumors. We next examined the effect of blocking the function of VEGFRs with specific antibodies raised against murine VEGFR-3 (mF4-31C1, anti-VEGFR-3) or murine VEGFR-2 (DC101, anti-VEGFR-2). Mice bearing intraprostatic tumors of CWR/RL cells were treated with either PBS (Ctrl), anti-VEGFR-3, or anti-VEGFR-2. Primary tumor growth, assessed by noninvasive optical imaging, was not significantly different for the anti-VEGFR-3 treated group compared with the control group (Fig. 5A). Conversely, a delay of ~4 days in average tumor signal was observed in the establishment of tumors in the anti-VEGFR-2 treated animals. At the end point on day 21, tumors from control and anti-VEGFR-3 treated animals were similar in size and gross morphologic appearance (Fig. 5B). By contrast, tumor volume of the anti-VEGFR-2 treated group was significantly reduced by ~70% compared with control tumors. The tumors also seemed to be pale and less vascular than the control and anti-VEGFR-3 treated tumors. The heightened bioluminescent signals registered in the anti-VEGFR-2 treated group, relative to the other two groups, may be related to the lower hemoglobin content because hemoglobin in blood is known to absorb photons emitted by luciferase (36).

We next evaluated the effect of therapeutic antibody treatment on tumor vasculature and metastasis. Tumor sections were

examined for differences in intratumoral blood and lymphatic vessel density (Fig. 5C). Whereas anti-VEGFR-2 treated tumors showed a 62% reduction in CD31+ vessel density, the reduction in Lyve-1+ lymphatic vessel density in the tumor margin was not statistically different from control. On the other hand, anti-VEGFR-3 treated tumors displayed no significant differences in CD31+ blood vessel density but a 50% reduction in Lyve-1+ lymphatics compared with control. Unexpectedly, we noted a reduction in lymphatic density in the normal prostate region, suggesting that VEGFR-3-mediated lymphangiogenesis in the surrounding normal tissue is influenced by tumor cells. Qualitatively, the lymphatic vessels in control and anti-VEGFR-2 treated tumors had significant lymphatic density at the tumor margin with vasculature extending into the tumor. Anti-VEGFR-3 treated tumors had a general lack of lymphatic vessels at the tumor margin, with isolated Lyve-1+ cells in the normal tissue. This phenomenon was similar to what we observed with sVEGFR-3.

The effect of therapeutic antibody treatment on nodal and systemic metastasis was analyzed by *ex vivo* optical imaging (Fig. 5D). Periaortic lymph nodes and lungs isolated from control animals exhibited extensive infiltration. Blocking VEGFR-2 signaling did not significantly diminish lymph node metastasis but resulted in a 6-fold reduction in signal in the lung. The most significant reduction in metastasis was observed in animals treated with anti-VEGFR-3 antibody, demonstrating 4-fold and 5-fold reductions in periaortic lymph node and lung metastasis, respectively. Overall, these data reinforce the critical role of lymphatics in the prostate tumor margin in metastasis. These data also reflect the significance of regional dissemination to lymph nodes in the potentiation of systemic metastasis. Additionally, these data highlight the importance of VEGFR-2 inhibition in controlling systemic metastasis without affecting lymph node metastasis.

Discussion

The notion that VEGF-C-induced lymphangiogenesis plays an important role in promoting regional lymph node metastasis is well supported in experimental models of breast cancer, as well as other solid cancers (37–39). Fewer studies have explored this issue in prostate cancer, although surveys of human tissue samples have linked activation of the VEGF-C/VEGFR-3 axis with poor clinical outcome. To study the process of prostate cancer dissemination *in vivo*, we developed human prostate cancer xenograft models (22) marked with bioluminescent luciferase reporter genes to facilitate tracking of metastases. In the poorly metastatic subcutaneous LAPC-9 xenograft model, tumoral lymphangiogenesis induced by VEGF-C and VEGF-C_{C156S}, a VEGFR-3 lymphangiogenic-selective mutant, directly promoted regional nodal metastasis, which was not observed in the tumors that received the dominant angiogenic drive of VEGF (Fig. 1). Moreover, the dramatic elevation of lymphatic dissemination promoted systemic dissemination to lungs. Thus, we used therapeutic strategies to parse the angiogenic and lymphangiogenic contributions to nodal and systemic dissemination. In the more aggressive subcutaneous CWR22Rv-1 model, suppression of the lymphangiogenic axis with the VEGF-C ligand trap resulted in clear diminution of tumoral lymphatics, lymph node, and lung metastasis (Fig. 2). On the other hand, shutdown of VEGF by shRNA diminished tumor growth and blood vasculature without a concomitant decline in nodal metastasis (Fig. 3).

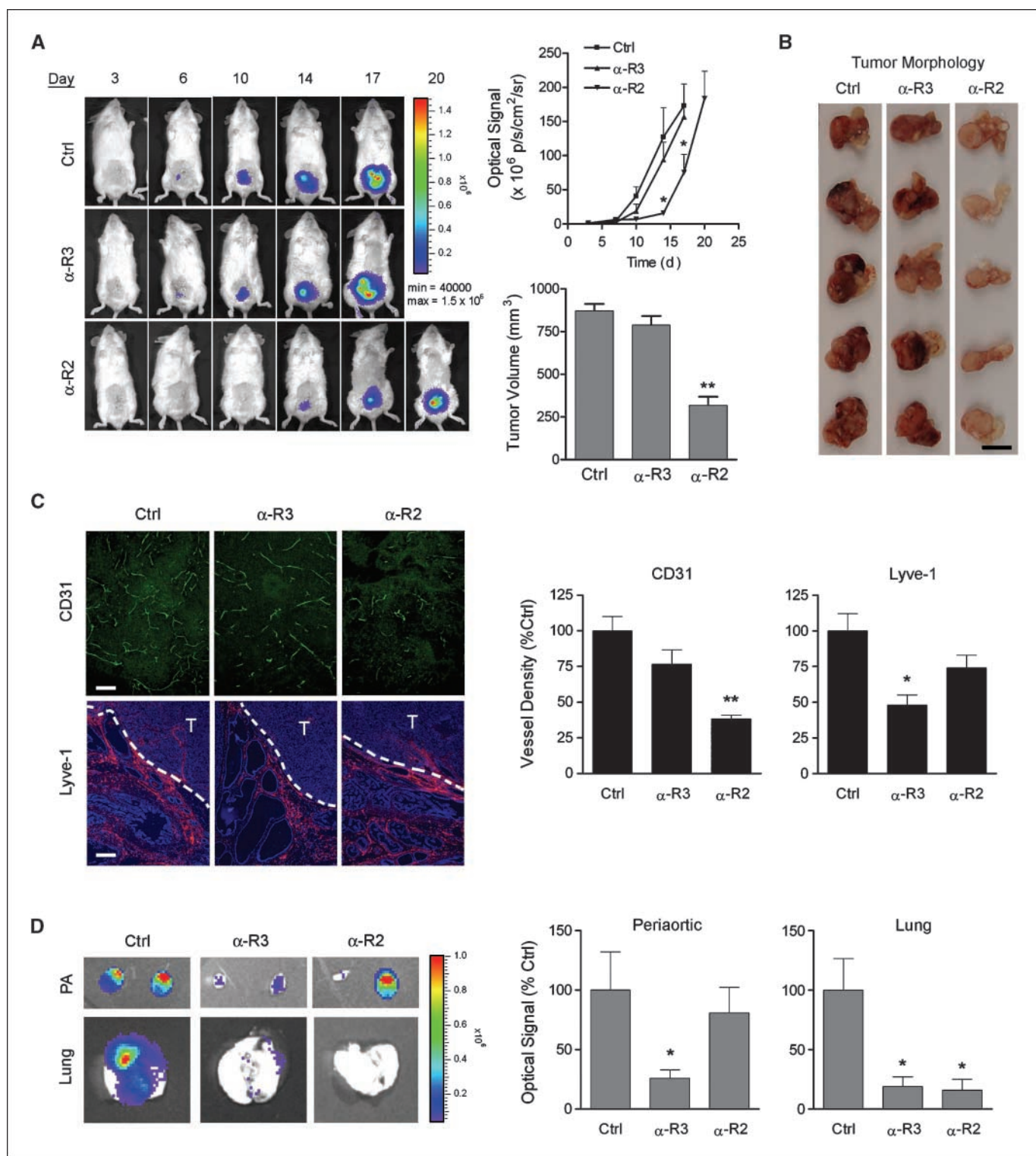


Figure 5. Orthotopic CWR22Rv-1 tumor growth characteristics with VEGFR-3 and VEGFR-2 blocking antibody treatment. CWR22Rv-1 tumors expressing *Renilla* luciferase were orthotopically implanted in SCID/*beige* mice ($n = 5$ per group). Treatment began 3 d postimplantation (Ctrl, PBS; α -R3, anti-VEGFR-3; α -R2, anti-VEGFR-2) with i.p. injections of 800 μ g/mouse of each antibody (100 μ L) every other day. **A**, representative images of optical signal in mice over the course of tumor growth for up to 20 d. All groups were sacrificed at comparable signal intensity (Ctrl and α -R3 were sacrificed at day 17; α -R2 were sacrificed at day 20). Averaged optical signal intensity over the course of tumor growth (*middle graph*) indicated a delay in optical signal in tumors of α -R2-treated animals. Upon sacrifice, tumors and adjoined seminal vesicles were removed, photographed, and measured. The α -R3-treated group displayed no significant differences in tumor volume compared with control, whereas α -R2 treatment reduced tumor volume and vascularity (**B**). **C**, tumors harvested from the respective treatment group were stained for blood (CD31) and lymphatic (*Lyve-1*) vessels (T, tumor). The treatment effects on vessel densities were measured and shown in the respective graph. **D**, periaortic lymph nodes (PA) and lungs from the respective treatment groups were dissected and imaged *ex vivo* for *Renilla* luciferase signal. Averaged luminescence signals from periaortic lymph nodes and lung are shown in respective graphs. Scale bars, 1 cm (**B**) and 20 μ m (**C**). Optical scale bars are in p/s/cm²/sr. Bars, SE. *, $P < 0.05$; **, $P < 0.01$. $n = 5$.

In orthotopic prostate tumor models, blockade of the lymphangiogenic axis by either VEGF-C ligand trap or VEGFR-3 blocking antibody resulted in a significant decrease in lymph node metastasis, but not in the growth of the prostatic tumor (Figs. 4 and 5). Conversely, abrogation of VEGFR-2 signaling with the anti-VEGFR-2 antibody significantly reduced tumor growth and blood vasculature without a corresponding reduction in nodal metastasis (Fig. 5). Collectively, these findings highlight the importance of controlling tumor lymphangiogenesis, not only to prevent regional lymph node spread but also in the suppression of systemic metastasis.

One of the findings of this study highlights the fact that the site of tumor implantation can have a significant influence on the metastatic behavior of prostate tumor xenografts. Clearly, unmodified LAPC-9 tumors lack the ability to disseminate when grafted in the subcutaneous site. The low metastatic potential of LAPC-9 tumors is due in part to its very low expression of VEGF-C, relative to the moderate and high levels expressed by CWR22Rv-1 and PC-3 tumor cells, respectively (22). In contrast, orthotopic LAPC-9 tumors readily metastasize to lymph nodes, without added vascular stimulus. In the stroma of the murine prostate gland, there are ample preexisting blood and lymphatic vessels, as well as inflammatory cells, which can provide additional growth factors that stimulate vasculature. The heightened angiogenic and lymphangiogenic potential in the prostatic microenvironment, compared with the subcutaneous site, could reflect reduced VEGF-C threshold levels required to promote lymphangiogenesis and nodal metastasis in prostate cancer.

The overall results presented here point to tumor lymphangiogenesis playing a more dominant role than angiogenesis in promoting lymph node and systemic metastasis in the LAPC-9 and CWR22Rv-1 prostate cancer models. An interesting corollary finding from this study is a direct connection between nodal and systemic metastasis. Previously, a report by Lin and colleagues showed that an adeno-associated virus expressing the sVEGFR-3 gene could inhibit lymph node and lung metastasis in a subcutaneous PC-3 prostate cancer model (40). Although this result points to the correlation between lymph node and lung metastasis, the low incidence of lung metastasis in the control arm of this previous study (<10%) precludes a firm conclusion on this issue. Three specific results reported here lend further support to the connection between lymph node and systemic metastasis. First, the lymphatic-specific VEGF-C_{C156S} promoted lymph node and lung metastasis without stimulating angiogenesis. Secondly, the development of lung metastasis was dependent on lymph node metastasis, meaning that no lung metastasis was observed in animals without nodal metastasis. Thirdly, the magnitude of lung and nodal metastasis directly correlated with each other in the four experimental groups, and the magnitude of lung signal was always lower than that in the lymph node. The latter two points suggest a sequential path of dissemination from lymph nodes to systemic sites.

The current antibody-based therapy showed that targeting VEGFR-3 signaling resulted in a dramatic reduction in nodal and systemic metastasis, whereas blocking VEGFR-2 dominantly diminished primary tumor growth. These results corroborate with the main findings of a recent report comparing VEGFR-2 and VEGFR-3 antibody therapies in an orthotopic breast cancer model (24). However, in that study, the authors observed a significant reduction in lymphangiogenesis with anti-VEGFR-2 treatment alone, which was not observed in our study. These opposing

findings may reflect differences in the tumor models used. The MDA-MB-435 breast xenograft model used in Roberts and colleagues study required VEGF-C overexpression to gain substantial metastases. In our case, we grafted the native CWR22Rv-1 tumor cells in the murine prostate gland. A recent study by Laakkonen and colleagues reported that VEGFR-3 blocking antibody therapy resulted in significant reduction in tumor vascular density and growth in a subcutaneous PC-3 prostate model (41). Different model systems may also be the reason that we observed a slight reduction in tumor angiogenesis without effecting tumor growth in the orthotopic CWR22Rv-1 model. Of interest, targeting the angiogenic VEGFR-2 axis did result in a significant suppression of lung metastasis, but not nodal metastasis. This finding implicates the contribution of tumor angiogenesis to lung metastasis. However, we need to be mindful that the suppressive effect on lung metastasis was reached in the context of a significant reduction in primary tumor growth. In contrast, the unabated nodal dissemination would suggest that the VEGFR-2 axis is not a critical component of lymphatic metastasis in our model.

A recent study by Wong and colleagues concluded that prostate tumor lymphangiogenesis is not required for lymph node metastasis (23). By genetic modulation with VEGF-C small interfering RNA or sVEGFR-3, they effectively down-regulated the intratumoral lymphatics in an orthotopic PC-3 xenograft model. Given a lack of suppression of nodal metastasis by these manipulations, they concluded that lymphangiogenesis was unnecessary for prostate cancer lymphatic metastasis (23). However, in this study, intratumoral lymphatics were equated to tumoral lymphangiogenesis. Yet, prior studies show that tumors often have elevated interstitial fluid pressure leading to collapsed and nonfunctional lymphatics within the tumor (42, 43). Instead, functional lymphatics in the tumor margin were sufficient to promote lymph node metastasis (43). In fact, the marginal lymphatics in the tumor periphery were not diminished by the inhibitory treatment in Wong and colleagues study. In the two orthotopic prostate tumor models studied here, we observed elaborate lymphatic vasculatures within the stroma of the normal prostatic region that extended into the tumor margin (marginal lymphatics) and a general lack of patent lymphatic vessels within the tumor. The sVEGFR-3 expressing tumors and the anti-VEGFR-3 treated tumors displayed a reduction in the marginal lymphatics at the prostatic and tumoral interphase. Moreover, they also seemed to take on less invasive characteristics. Instead of being elongated and interconnected as observed in the control tumors, the Lyve-1+ lymphatics in the treated tumors were isolated and less elaborate. These findings suggest that marginal lymphatics could likely be the conduit for the lymphatic route of tumor dissemination in prostate cancer.

In this study, we were able to distinguish the contributions of angiogenesis and lymphangiogenesis to tumor growth and dissemination. Treatment that can target both vascular axes, in combination with current therapeutic modalities, such as radiation therapy, prostatectomy, and hormone therapy, would be a rational approach to develop effective therapy to manage the most aggressive types of prostate cancer. An unresolved issue in applying antimetastatic therapies is the timing of administration. When is it too late to initiate the treatment? What is the appropriate time to stop the treatment? These critical questions can be addressed with a prostate cancer-specific molecular imaging modality. We are actively developing strategies based on the clinically relevant

positron emission tomography imaging for this purpose. Very recently, we were able to use a prostate-restricted gene expression vector to specifically detect nodal metastasis of prostate cancer (44). We remain hopeful that integrating molecular imaging to guide targeted therapies will improve the clinical outcome of patients with metastatic prostate cancer in the near future.

Disclosure of Potential Conflicts of Interest

B. Pytowski: Ownership interest, ImClone systems. The other authors declared no potential conflicts of interest.

References

- Jemal A, Siegel R, Ward E, et al. Cancer statistics, 2008. *CA Cancer J Clin* 2008;58:71–96.
- Roehl KA, Han M, Ramos CG, Antenor JA, Catalona WJ. Cancer progression and survival rates following anatomical radical retropubic prostatectomy in 3,478 consecutive patients: long-term results. *J Urol* 2004;172:910–4.
- Allaf ME, Palapattu GS, Trock BJ, Carter HB, Walsh PC. Anatomical extent of lymph node dissection: impact on men with clinically localized prostate cancer. *J Urol* 2004;172:1840–4.
- D'Amico AV, Whittington R, Malkowicz SB, et al. Pretreatment nomogram for prostate-specific antigen recurrence after radical prostatectomy or external-beam radiation therapy for clinically localized prostate cancer. *J Clin Oncol* 1999;17:168–72.
- Folkman J, Merler E, Abernathy C, Williams G. Isolation of a tumor factor responsible for angiogenesis. *J Exp Med* 1971;133:275–88.
- Ferrara N, Gerber HP, Lecouter J. The biology of VEGF and its receptors. *Nat Med* 2003;9:669–76.
- Carmeliet P. Angiogenesis in health and disease. *Nat Med* 2003;9:653–60.
- Klement G, Baruchel S, Rak J, et al. Continuous low-dose therapy with vinblastine and VEGF receptor-2 antibody induces sustained tumor regression without overt toxicity. *J Clin Invest* 2000;105:R15–24.
- Lee CG, Heijn M, di Tomaso E, et al. Anti-Vascular endothelial growth factor treatment augments tumor radiation response under normoxic or hypoxic conditions. *Cancer Res* 2000;60:5565–70.
- Jeltsch M, Kaipainen A, Joukov V, et al. Hyperplasia of lymphatic vessels in VEGF-C transgenic mice. *Science* 1997;276:1423–5.
- Veikkola T, Jussila L, Makinen T, et al. Signalling via vascular endothelial growth factor receptor-3 is sufficient for lymphangiogenesis in transgenic mice. *EMBO J* 2001;20:1223–31.
- He Y, Kozaki K, Karpanen T, et al. Suppression of tumor lymphangiogenesis and lymph node metastasis by blocking vascular endothelial growth factor receptor 3 signaling. *J Natl Cancer Inst* 2002;94:819–25.
- Mattila MM, Ruohola JK, Karpanen T, Jackson DG, Alitalo K, Harkonen PL. VEGF-C induced lymphangiogenesis is associated with lymph node metastasis in orthotopic MCF-7 tumors. *Int J Cancer* 2002;98:946–51.
- Mandriota SJ, Jussila L, Jeltsch M, et al. Vascular endothelial growth factor-C-mediated lymphangiogenesis promotes tumour metastasis. *EMBO J* 2001;20:672–82.
- Nagy JA, Vasile E, Feng D, et al. Vascular permeability factor/vascular endothelial growth factor induces lymphangiogenesis as well as angiogenesis. *J Exp Med* 2002;196:1497–506.
- Bjorn Dahl MA, Cao R, Burton JB, et al. Vascular endothelial growth factor-a promotes peritumoral

- lymphangiogenesis and lymphatic metastasis. *Cancer Res* 2005;65:9261–8.
- Hirakawa S, Kodama S, Kunstfeld R, Kajiya K, Brown LF, Detmar M. VEGF-A induces tumor and sentinel lymph node lymphangiogenesis and promotes lymphatic metastasis. *J Exp Med* 2005;201:1089–99.
- Zeng Y, Opekin K, Baldwin ME, et al. Expression of vascular endothelial growth factor receptor-3 by lymphatic endothelial cells is associated with lymph node metastasis in prostate cancer. *Clin Cancer Res* 2004;10:5137–44.
- Yang J, Wu HF, Qian LX, et al. Increased expressions of vascular endothelial growth factor (VEGF), VEGF-C and VEGF receptor-3 in prostate cancer tissue are associated with tumor progression. *Asian J Androl* 2006;8:169–75.
- Jennbacken K, Vallbo C, Wang W, Damber JE. Expression of vascular endothelial growth factor C (VEGF-C) and VEGF receptor-3 in human prostate cancer is associated with regional lymph node metastasis. *Prostate* 2005;65:110–6.
- Roma AA, Magi-Galluzzi C, Kral MA, Jin TT, Klein EA, Zhou M. Peritumoral lymphatic invasion is associated with regional lymph node metastases in prostate adenocarcinoma. *Mod Pathol* 2006;19:392–8.
- Brakenhielm E, Burton JB, Johnson M, et al. Modulating metastasis by a lymphangiogenic switch in prostate cancer. *Int J Cancer* 2007;121:2153–61.
- Wong SY, Haack H, Crowley D, Barry M, Bronson RT, Hynes RO. Tumor-secreted vascular endothelial growth factor-C is necessary for prostate cancer lymphangiogenesis, but lymphangiogenesis is unnecessary for lymph node metastasis. *Cancer Res* 2005;65:9789–98.
- Roberts N, Kloos B, Cassella M, et al. Inhibition of VEGFR-3 activation with the antagonistic antibody more potently suppresses lymph node and distant metastases than inactivation of VEGFR-2. *Cancer Res* 2006;66:2650–7.
- An DS, Xie Y, Mao SH, Morizono K, Kung SK, Chen IS. Efficient lentiviral vectors for short hairpin RNA delivery into human cells. *Hum Gene Ther* 2003;14:1207–12.
- Sato M, Figueiredo ML, Burton JB, et al. Configurations of a two-tiered amplified gene expression system in adenoviral vectors designed to improve the specificity of *in vivo* prostate cancer imaging. *Gene Ther* 2008;15:883–93.
- Loening AM, Gambhir SS. AMIDE: a free software tool for multimodality medical image analysis. *Mol Imaging* 2003;2:131–7.
- Pytowski B, Goldman J, Persaud K, et al. Complete and specific inhibition of adult lymphatic regeneration by a novel VEGFR-3 neutralizing antibody. *J Natl Cancer Inst* 2005;97:14–21.
- Witte L, Hicklin DJ, Zhu Z, et al. Monoclonal antibodies targeting the VEGF receptor-2 (Flk1/KDR)

- as an anti-angiogenic therapeutic strategy. *Cancer Metastasis Rev* 1998;17:155–61.
- Cao R, Brakenhielm E, Pawliuk R, et al. Angiogenic synergism, vascular stability and improvement of hind-limb ischemia by a combination of PDGF-BB and FGF-2. *Nat Med* 2003;9:604–13.
- Klein KA, Reiter RE, Redula J, et al. Progression of metastatic human prostate cancer to androgen independence in immunodeficient SCID mice. *Nat Med* 1997;3:402–8.
- Joukov V, Kumar V, Sorsa T, et al. A recombinant mutant vascular endothelial growth factor-C that has lost vascular endothelial growth factor receptor-2 binding, activation, and vascular permeability activities. *J Biol Chem* 1998;273:6599–602.
- Holleran JL, Miller CJ, Culp IA. Tracking micrometastasis to multiple organs with lacZ-tagged CWR22R prostate carcinoma cells. *J Histochem Cytochem* 2000;48:643–51.
- De Wever O, Mareel M. Role of tissue stroma in cancer cell invasion. *J Pathol* 2003;200:429–47.
- Joukov V, Pajusola K, Kaipainen A, et al. A novel vascular endothelial growth factor, VEGF-C, is a ligand for the Flt4 (VEGFR-3) and KDR (VEGFR-2) receptor tyrosine kinases. *EMBO J* 1996;15:290–8.
- Zhao H, Doyle TC, Coquoz O, Kalish F, Rice BW, Contag CH. Emission spectra of bioluminescent reporters and interaction with mammalian tissue determine the sensitivity of detection *in vivo*. *J Biomed Opt* 2005;10:41210.
- Skobe M, Hawighorst T, Jackson DG, et al. Induction of tumor lymphangiogenesis by VEGF-C promotes breast cancer metastasis. *Nat Med* 2001;7:192–8.
- Karpanen T, Egeblad M, Karkkainen MJ, et al. Vascular endothelial growth factor C promotes tumor lymphangiogenesis and intralymphatic tumor growth. *Cancer Res* 2001;61:1786–90.
- Alitalo K, Carmeliet P. Molecular mechanisms of lymphangiogenesis in health and disease. *Cancer Cell* 2002;1:219–27.
- Lin J, Lalani AS, Harding TC, et al. Inhibition of lymphogenous metastasis using adeno-associated virus-mediated gene transfer of a soluble VEGFR-3 decoy receptor. *Cancer Res* 2005;65:6901–9.
- Laakkonen P, Waltari M, Holopainen T, et al. Vascular endothelial growth factor receptor 3 is involved in tumor angiogenesis and growth. *Cancer Res* 2007;67:593–9.
- Jain RK. Barriers to drug delivery in solid tumors. *Sci Am* 1994;271:58–65.
- Padera TP, Kadambi A, di Tomaso E, et al. Lymphatic metastasis in the absence of functional intratumor lymphatics. *Science* 2002;296:1883–6.
- Burton JB, Johnson M, Sato M, et al. Adenovirus mediated gene expression imaging to directly detect sentinel lymph node metastasis of prostate cancer. *Nat Med* 2008;14:882–8.

Acknowledgments

Received 4/22/2008; revised 6/3/2008; accepted 6/15/2008.

Grant support: National Cancer Institute Specialized Programs of Research Excellence program P50 CA092131, Prostate Cancer Foundation (L. Wu), and Margaret E. Early Medical Trust award (L. Wu). J. Burton is supported by Department of Defense grant CDMRP 07-1-0064 (prostate cancer predoctoral training grant). S. Priceman is supported by the career developmental program of University of California at Los Angeles ICMIC grant (P50 CA86306 to H.R. Herschman).

The costs of publication of this article were defrayed in part by the payment of page charges. This article must therefore be hereby marked *advertisement* in accordance with 18 U.S.C. Section 1734 solely to indicate this fact.

We thank Jimmy Ou and David Stout in Crump Institute of Molecular Imaging for the technical support.